Archives of Hydro-Engineering and Environmental Mechanics
Vol. 52 (2005), No. 4, pp. 303–320

A Turbulence Model for 3-D Flows with Anisotropic Structure of Turbulence

Włodzimierz Czernuszenko*, Alexy Rylov**

*Polish Academy of Sciences, Institute of Geophysics,
Ks. Janusza 64, 01-452 Warsaw, Poland, e-mail: wczer@igf.edu.pl
**Institute for Water and Environmental Problems,
Papanintsev 105, Barnaul, Russia, e-mail: raa05@yandex.ru

(Received May 04, 2005; revised July 07, 2005)

Abstract

A new turbulence model for flows in open channels with compound cross-sections is presented. The structure of turbulence in these channels can be anisotropic. This structure is described by the turbulent stress tensor that is presented here as the sum of two tensors, namely, normal and shear stress tensors. The normal and shear turbulent stresses are expressed by the turbulence intensities and the mixing length tensor (MLT), respectively. The turbulence intensities can be learned from measurements or another suitable approaches. One such approach that allows calculating the main component of the normal stresses is presented in the paper. The components of MLT are defined based on a new concept of generic mixing length (GML). The generic mixing length is assumed to depend on both distances; from the nearest wall and from the water surface. To demonstrate how the new model works the basic hydrodynamic equations (parabolic approximation of Reynolds equations) together with the turbulence model are solved. The well-known Patankar and Spalding (1972) algorithm was used when solving these equations. A series of numerical simulations were performed for different components of MLT and different channel geometries.

Key words: 3D flow, mathematical model, numerical simulation, open channel flow, turbulence model

1. Introduction

Flows in an open channel with compound cross section are considered here to be stationary turbulent flows of Newtonian fluid, uniform in a longitudinal direction. Flow conditions in these channels lead to a complex 3D turbulent structure, which is generated by the channel bottom. Due to non-regular cross section the slope of the tangent to the channel bottom with respect to horizontal plane varies in different points of the channel bottom. This causes velocity distribution in cross section to be rather complicated with anisotropic structure of turbulence.

To describe this three-dimensional (3D) highly complicated velocity field, very advanced mathematical models have been developed, e.g. the algebraic stress model (ASM), see for example (Krishnappan and Lau 1986) or (Naot et al 1993), or the complete Reynolds-stress-transport model of turbulence, see for example (Cokljat and Younis 1995). Unfortunately, these 3D models require a large number of empirical constants which means they are not very useful for engineering purposes. These models, despite their achievements in description of the 3D-velocity field, are not suitable for engineers in calculating velocity and other flow characteristics in compound channel flows. For example, the above-mentioned algebraic stress model comprises 11 differential equations with 7 empirical coefficients and two empirical functions. The set of equations contains three momentum equations and continuity equation governing the three-dimensional mean motion and the mean pressure, two transport equations for the energy of turbulence and their dissipation and six algebraic equations representing the anisotropy by means of the Reynolds stresses given in terms of the turbulence energy, dissipation and mean velocity gradients. In so complicated a set of differential equations it is impossible to realize the roles of all those empirical coefficients and functions involved. Furthermore, applying any calibration procedure for these models is doubtful, and in turn, using these models for other channels is questionable. Engineers need a model that is easy to understand, simple to calibrate and reasonably good.

The three-dimensional turbulent models for typical open channel flows, that match all engineering demands are rather scarce. The main goal of this paper is to present a model that takes into account the origin of turbulence, the anisotropy of turbulence structure and at the same time is reasonably good and simple to calibrate. The model is based on a new, modified 3D mixing length hypothesis (MLH) developed by Czernuszenko and Rylov (2000). In this modification the normal turbulent stresses are treated as anisotropic and the model for these stresses is presented. The model for shear stresses is redefined compared with the first version of 3D MLH (see Czernuszenko and Rylov 2000). Now these two sub-models, for normal and shear stresses, are clearer and easy to adopt for numerical procedure that solves basic hydrodynamic equations.

Presented turbulence model can be used for compound open channels with any cross section the bed curve of which holds a property: a vertical line segment connecting each inner flow point to the corresponding surface point lies entirely inside the cross section. In this case the normal and shear turbulent stresses can be defined first in the local coordinate system and then transformed into the global coordinate system in which the hydrodynamics equations are written. It is also shown how to define the local and global coordinate systems and define the transformation between both of them.

2. Basic Hydrodynamic Equations

Three-dimensional, steady and uniform turbulent flow in an open channel is governed by the Reynolds-averaged Navier-Stokes equations. The continuity and momentum equations for incompressible turbulent flows may be written in the Cartesian tensor notation in the forms:

– continuity equation

$$\frac{\partial U_i}{\partial x_i} = 0, \tag{1}$$

– momentum equations

$$U_j \frac{\partial U_i}{\partial x_j} = -\frac{1}{\rho}\frac{\partial p}{\partial x_i} + F_i - \frac{\partial}{\partial x_j}\left(\overline{u_i u_j} - \nu \frac{\partial U_i}{\partial x_j}\right), \tag{2}$$

where U_i is the i-th component of the time average velocity ($i = 1, 2, 3$), p is the pressure, ρ is density and $\mathbf{F} = (g \sin\alpha, g \cos\alpha, 0)$. A notation of x for horizontal (longitudinal), y for vertical (downwards) and z for lateral coordinates as well as U, V, W for corresponding velocity components will also be used in the paper.

3. Turbulence Model

A new turbulence model is an extended version of models presented by Czernuszenko and Rylov (2000) and Czernuszenko and Rylov (2002). The model describes the turbulence structure in the case of anisotropic normal turbulent stresses, as well as the anisotropic shear stresses in the form of:

$$-\rho\,\overline{u_i u_j} = \begin{cases} -\rho\,\overline{u_i^2} & \text{for} \quad i = j, \\ \\ \dfrac{1}{2}\,\rho\,\left(l_{ik}^2 D_{kj} + l_{jk}^2 D_{ki}\right) S & \text{for} \quad i \neq j, \end{cases} \tag{3}$$

where: u_i is the i-component of turbulent velocity vector, l_{ij} – the mixing length tensor, D_{ij} – the deformation rate tensor

$$D_{ij} = \frac{\partial U_i}{\partial x_j} + \frac{\partial U_j}{\partial x_i} \tag{4}$$

and quantity S are defined by the formula (Czernuszenko and Rylov 2000)

$$S = \sum_{i,k} \left|\frac{\partial U_i}{\partial x_k}\right|. \tag{5}$$

For the open channel flows the right-hand sum in Eq. (5) may be reduced to two terms containing derivatives of streamwise velocities in lateral and vertical directions, respectively. The other terms in the sum above containing the lateral

and vertical components of the mean velocity vector do not exceed 1–2% of the streamwise component. The upper line on the right-hand side of Eq. (3) represents the normal turbulent stresses. The shear stresses are written in the second line of Eq. (3).

For 2-D flows, since $S = |dU/dy|$, $D_{xy} = D_{yx} = dU/dy$ and $D_{xx} = D_{xz} = D_{yy} = D_{zy} = 0$, the shear stress takes the form (from Eq. 3):

$$-\rho\,\overline{u_x u_y} = \frac{1}{2}\rho\left(l_{xx}^2 + l_{yy}^2\right)\left|\frac{dU}{dy}\right|\frac{dU}{dy}. \tag{6}$$

If MLT is isotropic, Eq. (6) turns into the Prandtl's mixing length formula (see Schlichting 1955). This is the reason why the turbulence model (Eq. 3) can be called the 3D mixing length hypothesis. This hypothesis needs to specify the normal and shear turbulence stresses at any point of the cross-section for prescribing the total turbulent stress tensor. One can use Eq. (6) to define an effective eddy viscosity in 2D uniform, turbulent flows as

$$\nu_{effective} = \frac{1}{2}\left(l_{xx}^2 + l_{yy}^2\right)\left|\frac{dU}{dy}\right|. \tag{7}$$

3.1. Normal Turbulent Stresses

Components of normal turbulent stresses can be calculated or measured. There are three universal functions for calculation normal stresses in 2D flows given by Nezu and Nakagawa (1993). These functions define the turbulence intensities depending on distance from the bottom in the form:

$$\frac{\sqrt{\overline{u_i^2}}}{U_*} \equiv \frac{u_i'}{U_*} = D_i \exp\left(-C_k\xi\right) \tag{8}$$

where D_i ($i = 1, 2, 3$) and C_k are empirical constants and ξ is a non-dimensional distance from the wall.

The precise measurements of velocity in 2D open channel flows allow to evaluate the empirical constants in equations (8) as follows: $C_k = 1, D_1 = 2.30$, $D_2 = 1.27$ and $D_3 = 1.63$ (see Nezu and Nakagawa 1993). Eqs. (8) with above-mentioned coefficients fit the measurement data quite well especially in the region $0.1 < \xi < 0.8$ (Nezu and Nakagawa 1993). It is worth noting that the longitudinal intensity is larger than transverse ones and suitable ratios are: $v'/u' = 0.55$ and $w'/u' = 0.71$. It is assumed that Eq. (8) could be applied to any point of the channel cross-section. In the case of 3D flow, the non-dimensional distance from the wall is redefined as follows,

$$\xi = \frac{d_1}{d_1 + d_2}, \tag{9}$$

where d_1 and d_2 are distances from the nearest wall and water surface, respectively (Fig. 1).

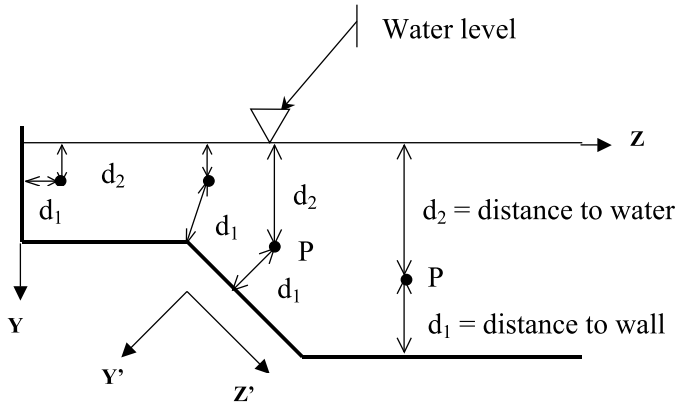

Fig. 1. Distances from point P to water surface and walls for different positions of point P in the channel cross-section. (Y, Z) – global coordinate system, (Y', Z') – local coordinate system

3.2. Shear Turbulent Stresses

To calculate the shear stresses the MLT, as well as the deformation tensor, should be specified. The components of MLT are defined first in the Cartesian coordinate system in which the MLT has a diagonal form. This coordinate system is called the local coordinate system (LCS). It is well-known that LCS in which tensor l_{ij} has only three non-zero components l_{11}, l_{22}, and l_{33} always exists. Below, these three components are referred to as l_x, l_y, and l_z respectively. To define these components a generic mixing length is defined as an analogue of Prandtl's mixing length, but established in the whole cross-section of a channel in the form:

$$l_G(P) = (d_1 + d_2)\ \kappa\sqrt{1-\xi}\ \left(\frac{1}{\xi} + \pi\ \Pi\ \sin(\pi\xi)\right)^{-1}\ \Gamma(\xi), \tag{10}$$

where: κ is the Karman constant, Π is the Coles wake coefficient, $\Gamma(\xi)$ is van Driest's damping function and ξ is defined by Eq. (9). The wake coefficient for open channel turbulent flows is near zero at moderate Reynolds number and this value is taken for further considerations. Van Driest's function shows that the mixing length does not vary linearly with distance from the wall. It takes into account the effect of lowering mixing length very close to the wall (see e.g. Launder, Spalding 1974). In our case, it is assumed that $\Gamma(\xi)$ is constant and equal to 1.

It is worth noting that the mixing length calculated from Eq. (10) for flow points located far away from the side walls, gives the same mixing length as the

formula for Prandtl's mixing length given by Nezu and Rodi (1986). Close to walls (vertical or inclined) the depth is not equal to the sum of d_1 and d_2. Based on the generic mixing length the main components of the mixing length tensor can be defined in the following way

$$l_x = pl_G\ , \quad l_y = q_y l_x\ , \quad l_z = q_z l_x \tag{11}$$

where p, q_y and q_z are empirical, positive coefficients. Bearing in mind that Eq. (10) should converge to Prandtl's formula in the middle zone of the channel, it results in constraints on the above-mentioned coefficients

$$p^2(1+q_y^2) = 2 \quad \text{for} \quad p < \sqrt{2}. \tag{12}$$

The decomposition defined by Eq. (11) invokes 3D mixing length ellipsoid with main axes l_x, l_y and l_z. This means that the scalar mixing length in Prandtl's approach becomes the mixing length ellipse in 2D flow or ellipsoid in the 3D case.

Prandtl mixing length can characterize an average size of turbulent eddies. Near walls this size is close to zero, and near the water surface it is the largest. The largest vertical size of turbulent eddies is an order of the flow depth, but the largest mixing length calculated from Eq. (10) is about 1/7 of the depth. Presumably, there is a relation between the mixing length ellipsoid and size of turbulent eddies. Thus, decomposition of l_{3D} into three main components of the mixing length tensor gives in turn: decomposition of spherical turbulent eddies into 3D ellipsoid eddies. Measurement data show that turbulent eddies in open channel flows are extended in a longitudinal direction, so one can expect $q_y < 1$ and $p > 1$. Eqs. (11) and (12) enable estimation of the components of the mixing length tensor when the generic mixing length, as well as the two coefficients p and q_z are known.

4. Global Coordinate System

Cartesian coordinate system in which basic hydrodynamics equations are written, is called the global coordinate system (GCS). Formulae (8) and (10) enable calculating the intensities of turbulence and components of MLT only in LCS, i.e. in the coordinate system where these quantities form diagonal tensors. Generally, the coordinate axes of LCS have a different direction from those of the global coordinate system (GCS). It depends on the geometry of the channel, whether GCS and LCS coordinate axes actually have the same directions or not. Both coordinate systems rigidly rotate to each other. The rotation is specified by an angle between adequate axes of these systems. Denote the angle by α, then transformation will be described by the matrix

$$\mathbf{T} = \begin{bmatrix} 1 & 0 & 0 \\ 0 & \cos\alpha & \sin\alpha \\ 0 & -\sin\alpha & \cos\alpha \end{bmatrix}. \tag{13}$$

This means, if a point P has coordinates (x_1', x_2', x_3') in LCS and (x_1, x_2, x_3) in GCS, then these coordinates are transformed as

$$[\mathbf{x}] = \mathbf{T}[\mathbf{x}'], \tag{14}$$

where column vectors $[\mathbf{x}]$ and $[\mathbf{x}']$ refer to the point coordinates in GCS and LCS, respectively. Further in the text, the coordinates of points or vectors, as well as the components of MLT in LCS will be primed, but in GCS these quantities will appear without a prime. Please note that so far, the coordinates of the local coordinate system have been used without prime.

The mixing length tensor is a second order tensor. In LCS it has components l_{ij}' defined by Eqs. (10) and (11). The components of this tensor in GCS, which is rotated about angle α relative to LCS, are denoted by l_{ij} and read (Aris 1989):

$$\mathbf{L} = \mathbf{T}\mathbf{L}'\mathbf{T}^{-1} \text{ where } \mathbf{L} = [l_{ij}], \mathbf{L}' = [l_{ij}']. \tag{15}$$

Combining Eqs. (10) and (15) gives an explicit formula for components of MLT in GCS

$$L = \begin{bmatrix} l_x' & 0 & 0 \\ 0 & l_y' \cos^2\alpha + l_z' \sin^2\alpha & \dfrac{\sin 2\alpha}{2}\left(l_z' - l_y'\right) \\ 0 & \dfrac{\sin 2\alpha}{2}\left(l_z' - l_y'\right) & l_z' \cos^2\alpha + l_y' \sin^2\alpha. \end{bmatrix}. \tag{16}$$

It is easy to notice that when $l_x' = l_y' = l_z'$ the above formula gives an isotropic MLT. For the angle $\alpha = 90^\circ$ the components of MLT form a diagonal matrix. Also for $\alpha = 45^\circ$ MLT takes a rather simple form.

While considering the normal turbulent stress tensor, its components in LCS will be assumed to be known and they will be denoted by a prime. Here the same usage of a prime is applied as for MLT, i.e. components of normal stresses in LCS will be primed, and in GCS these quantities will appear without a prime. In LCS the normal turbulent stress tensor is as follows

$$\mathrm{N}' = \begin{bmatrix} \rho\,\overline{\left(u_1^2\right)'} & 0 & 0 \\ 0 & \rho\,\overline{\left(u_2^2\right)'} & 0 \\ 0 & 0 & \rho\,\overline{\left(u_3^2\right)'} \end{bmatrix}. \tag{17}$$

Having components of the normal turbulence stresses in LCS, one can calculate them in GCS in the same way as components of MLT, namely

$$\mathbf{N} = \mathbf{T}\,\mathbf{N}'\,\mathbf{T}^{-1}. \tag{18}$$

After some algebra one can obtain the following formulae for the main components of normal turbulent stress tensor in GCS:

$$\begin{aligned} \overline{u^2} &= \overline{(u^2)'}, \\ \overline{v^2} &= \overline{(v^2)'}\cos^2\alpha + \overline{(w^2)'}\sin^2\alpha, \\ \overline{w^2} &= \overline{(v^2)'}\sin^2\alpha + \overline{(w^2)'}\cos^2\alpha. \end{aligned} \tag{19}$$

In the above equations density is omitted for simplicity.

5. Hydrodynamic Model

Consider an open channel that is tilted in a longitudinal direction, the bed slope is defined by an angle α and walls are smooth or rough. The flow is supposed to be steady with average velocity components (U, V, W) directed in x, y and z directions, respectively. It is assumed that the turbulent transport of momentum in the x-direction is negligible. Therefore, the terms involving second derivatives with respect to x are negligible. This kind of flow is usually called parabolic in the longitudinal direction. The basic equations describing the 3D-velocity field in open channel flows are the continuity (1) and momentum equations (2). Substituting Eq. (3) into Eq. (2) and neglecting higher order terms one can obtain momentum equations in the form:

$$\begin{aligned} &\frac{\partial U^2}{\partial x} + \frac{\partial VU}{\partial y} + \frac{\partial WU}{\partial z} + \frac{1}{\rho}\frac{\partial p}{\partial x} = g\sin\theta + \frac{\partial}{\partial y}\left(\frac{1}{2}\left(l_x^2 + l_y^2\right)S\frac{\partial U}{\partial y}\right) + \\ &+\frac{\partial}{\partial y}\left(\frac{1}{2}l_{yz}^2 S\frac{\partial U}{\partial z}\right) + \frac{\partial}{\partial z}\left(\frac{1}{2}\left(l_x^2 + l_z^2\right)S\frac{\partial U}{\partial z}\right) + \frac{\partial}{\partial z}\left(\frac{1}{2}l_{yz}^2 S\frac{\partial U}{\partial y}\right), \end{aligned} \tag{20}$$

$$\begin{aligned} &\frac{\partial UV}{\partial x} + \frac{\partial V^2}{\partial y} + \frac{\partial WV}{\partial z} + \frac{1}{\rho}\frac{\partial p}{\partial y} = g\cos\theta + \frac{\partial}{\partial y}\left(-\overline{v^2}\right) + \\ &+\frac{\partial}{\partial y}\left(2Sl_y^2\frac{\partial V}{\partial y} + Sl_{yz}^2\left(\frac{\partial W}{\partial y} + \frac{\partial V}{\partial z}\right)\right) + \frac{\partial}{\partial z}\left(\frac{1}{2}S\left(l_y^2 + l_z^2\right)\left(\frac{\partial V}{\partial z} + \frac{\partial W}{\partial y}\right)\right), \end{aligned} \tag{21}$$

$$\begin{aligned} &\frac{\partial UW}{\partial x} + \frac{\partial VW}{\partial y} + \frac{\partial W^2}{\partial z} + \frac{1}{\rho}\frac{\partial p}{\partial z} = \frac{\partial}{\partial z}\left(-\overline{w^2}\right) + \\ &+\frac{\partial}{\partial y}\left[\left(\frac{S}{2}\left(l_y^2 + l_z^2\right)\right)\left(\frac{\partial V}{\partial z} + \frac{\partial W}{\partial y}\right)\right] + \frac{\partial}{\partial z}\left[Sl_{yz}^2\left(\frac{\partial V}{\partial z} + \frac{\partial W}{\partial y}\right) + 2Sl_z^2\frac{\partial W}{\partial z}\right], \end{aligned} \tag{22}$$

where p is the pressure, S is defined by Eq. (5), l_x, l_y, l_z and l_{yz} are functions of l_x', l_y', l_z' and can be found from Eq. (16).

The boundary conditions need to be specified along solid boundaries, water surface and up-stream cross-section bounding the calculation domain. Since parabolic flows are considered, boundary conditions do not need to be given at the downstream end of the calculation domain.

It is assumed that the flow is uniform with constant width and depth. The conditions at the solid boundaries were specified using wall functions technique proposed by Launder and Spalding (1974). According to this, the conditions are specified at a point near a wall which lies outside the laminar sublayer and satisfies $30 < U_* y_w/\nu < 100$. It is assumed that the shear stress and velocity at this grid point satisfy the logarithmic portion of the universal law of the wall

$$\frac{U_w}{U_*} = \frac{1}{\kappa} \ln \frac{y_w}{k_*} + A, \text{where} \begin{cases} \text{for smooth channels } k_* = \nu/U_*, \ A \equiv A_s = 5.5, \\ \text{for rough channels } k_* \equiv k_s, \ A \equiv A_r = 8.5, \end{cases} \tag{23}$$

where:

U_* – friction velocity,
y_w – distance from the wall,
ν – molecular viscosity,
A – constant coefficient and
k_s – the equivalent sand roughness for irregular surfaces.

The normal velocity components at the solid boundaries and free surface are set at zero. The free surface boundary conditions were specified following the approach of Rastogi and Rodi (1978), which considers free surface acting as a plane of symmetry. Therefore, the gradients of U and V in the y-direction are zeros. The condition at the initial cross section $x = 0$ for longitudinal velocity U was taken along with logarithmic distribution. Components V and W were set equal to zero.

To solve the above set of equations the numerical parabolic procedure known as the Patankar-Spalding algorithm is applied. It solves the set of the above equations for three components of velocity U, V, W at each forward step in a longitudinal direction. After having computed component U at the next x-step from the discrete form of Eq. (20), U is corrected to preserve the prescribed discharge. Then both V and W discrete analogues for Eqs. (21)–(22) are solved to get first approximation for these velocity components at the next x-point cross section. The last stage of solution procedure uses the V, W-values and adjusts them to satisfy the discrete continuity equation. It means that Eqs. (1, 21, 22) in their discrete form are combined to produce an equation for the pressure field in cross section. The pressure found allows computing residuals to correct secondary velocities. All linear systems, which appear in the discretization process, hold maximum principle

and therefore, they are stable while solving. The scheme uses a mixed pattern in approximation of convective terms in motion equations. Generally, it is of the second order but it degrades to first-order upwind scheme when secondary velocity components are comparable to U values. Fortunately, in the flow cases under consideration, the primary velocity component always dominates over secondary velocity values, and therefore, accuracy of the second order is asserted.

6. Numerical Simulations of Flows in Trapezoidal Compound Channel

The numerical simulations were performed for stationary, uniform turbulent flow in the straight, smooth compound channel. The channel is 52 cm wide at the water surface and widths of main channel and flood plane are 0.15 m and 0.075 m, respectively. The depths of main channel and flood plane are 0.11 m and 0.075 m, respectively. The longitudinal bed slope is 1.03×10^{-3} and the sidewalls are inclined under the angle of 45 degrees.

The main objective of the numerical simulations is to show the most important features of the presented turbulence model, like its ability to describe the primary velocity distributions as well as the secondary flows for different structure of turbulence. The structure was defined by the size of main components of the MLT or in other words by the relative magnitudes of coefficients p, q_y and q_z defined by Eq. (11). All cases of numerical simulations are displayed in Table 1.

Table 1. Numerical simulations for trapezoidal compound channel: l_x, l_y and l_z – main components of mixing length tensor, $\mathrm{Grad}_x\ p$ – the longitudinal mean pressure gradient and $Q_{\max} = (V^2 + W^2)^{0.5}_{\max}$

	Case 1 Figure 2	Case 2 Figure 3	Case 3 Figure 4	Case 4 Figure 5	Case 5 Figure 6
x – component	$l_x = l_G$	$l_x = 1.26 l_G$	$l_x = 1.38 l_G$	$l_x = l_G$	$l_x = l_G$
y – component	$l_y = l_x$	$l_y = 0.51 l_x$	$l_y = 0.22 l_x$	$l_y = l_x$	$l_y = l_x$
z – component	$l_z = l_x$	$l_z = 0.51 l_x$	$l_z = 0.22 l_x$	$l_z = 0.67 l_x$	$l_z = 1.45 l_x$
$\mathrm{Grad}_x\ p$ [N/m^2]	–3.1	–3.1	–3.1	2.8	3.9
$Q_{\max}$ [m/s]	0.0116	0.0144	0.0174	0.0126	0.0103
$U_{\max}$ [m/s]	0.345	0.345	0.345	0.34	0.339

6.1. Results of Numerical Simulations

For isotropic MLT the prime velocity contour is very regular with logarithmic profile in the channel centre (Case 1, Fig. 2a). The intensity of secondary flow is rather weak, $Q_{\max} = 0.0116$ m/s (see Fig. 2b). If the MLE is elongated in a longitudinal direction, i.e., l_x is twice (Case 2, Fig. 3a, b) and 4.5 times longer than l_y and l_z (Case 3, Fig. 4a, b), the prime velocity contour remains almost the same and the intensity of secondary flow increases to 0.0144 m/s and 0.0174 m/s, respectively (Fig. 3b and Fig. 4b). This behaviour is easy to explain by analyzing Eqs. (20), (21) and (22) as follows: the x-momentum equation remains the same

for any set of parameters p, q_y and q_z, provided that $q_y = q_z$ and Eq. (12) is valid. One can easily see from transversal components of momentum equations, that as both l_y and l_z decrease, the transversal eddy viscosities also decrease. It causes, in turn, the increase of transversal velocities and the intensity of secondary flow, namely from 0.0116 m/s (Case 1) via 0.0144 m/s (Case 2) to 0.0174 m/s (Case 3).

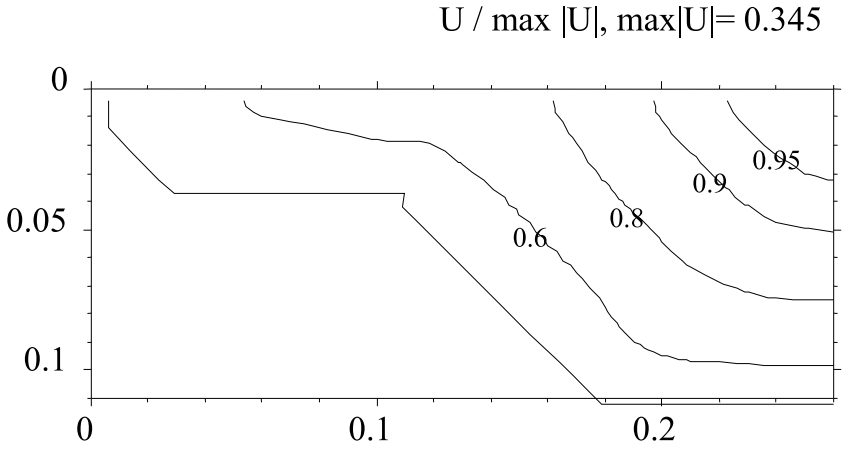

Fig. 2a. Prime velocity distribution for: $l_x = l_G, l_y = l_x, l_z = l_x$

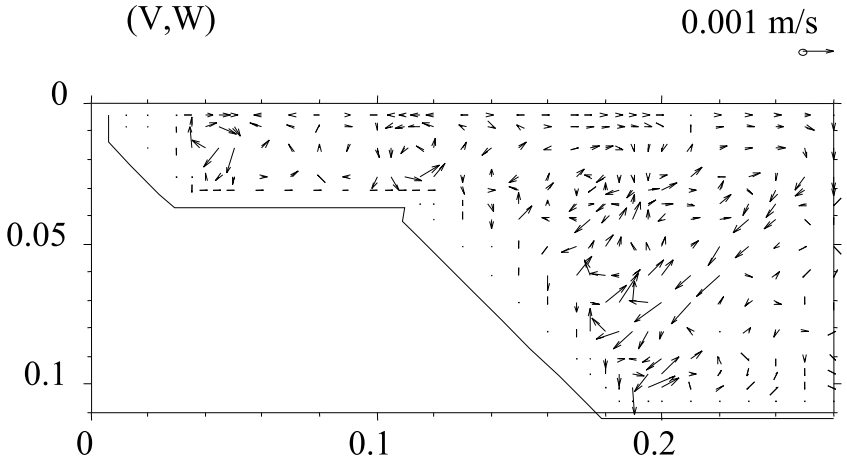

Fig. 2b. Secondary currents pattern for: $l_x = l_G, l_y = l_x, l_z = l_x$; $Q_{\max} = 0.0116$ m/s

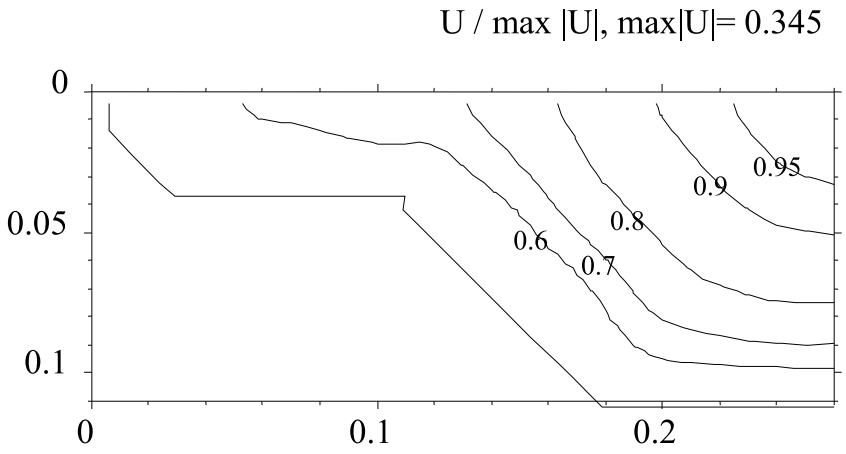

Fig. 3a. Prime velocity distribution for: $l_x = 1.26 l_G, l_y = 0.51 l_x, l_z = 0.51 l_x$

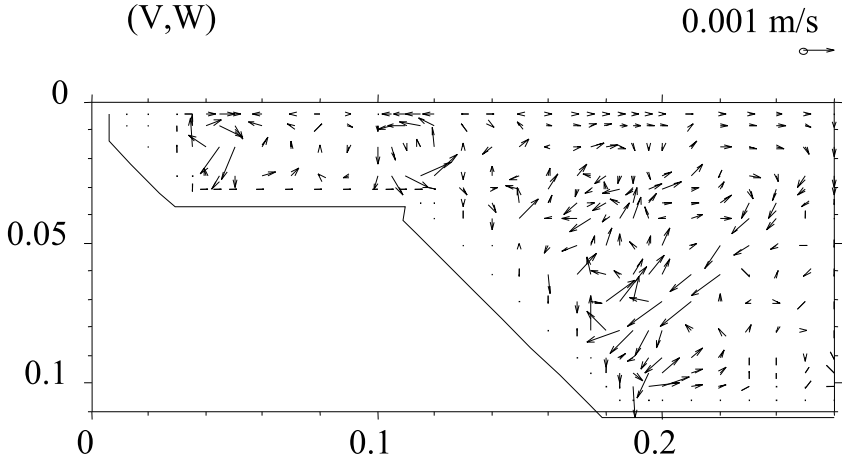

Fig. 3b. Secondary currents pattern for: $l_x = 1.26\, l_G, l_y = 0.51 l_x, l_z = 0.51 l_x$; $Q_{\max} = 0.0144$ m/s

The pressure gradient in x-direction is the same for these cases, and equals to –3.1 N/m^2. It means that the total viscosity influence (joint impact of all terms describing viscosity) in the x-momentum equation is almost the same. Thus, the prime velocity contours are the same in these cases.

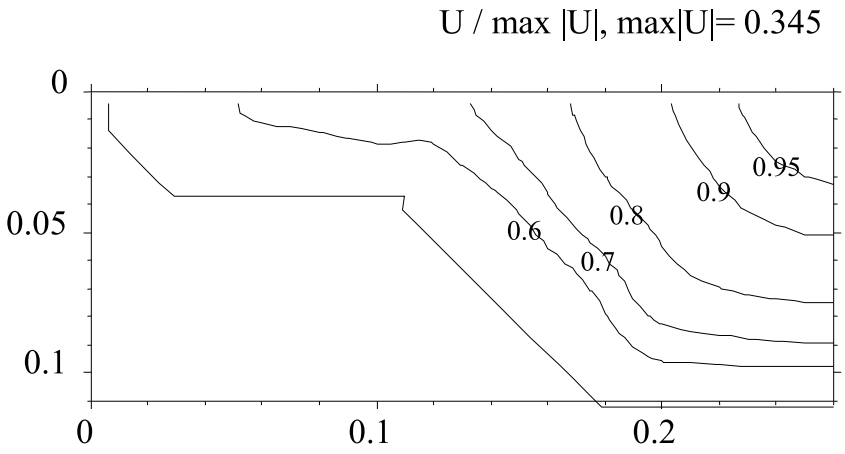

Fig. 4a. Prime velocity distribution for: $l_x = 1.38l_G, l_y = 0.22l_x, l_z = 0.22l_x$

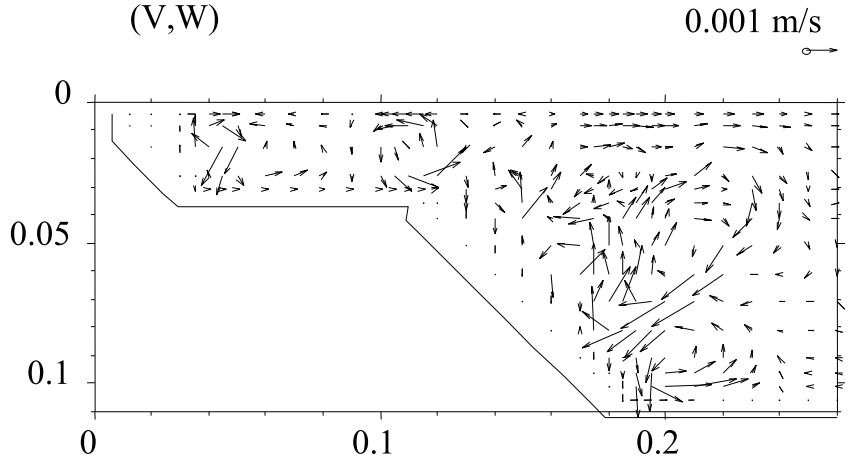

Fig. 4b. Secondary currents pattern for: $l_x = 1.38l_G$, $l_y = 0.22l_x, l_z = 0.22l_x$; $Q_{\max} = 0.0174$ m/s

Comparing three other cases, namely: $l_z : l_y = 0.67$ (Case 4, Fig. 5), $l_z : l_y = 1$ (Case 1, Fig. 2) and $l_z : l_y = 1.45$ (Case 5, Fig. 6) some differences in the results of numerical simulations are easy to notice (see Table 1). First of all, among the cases under consideration $\text{grad}_x p$ is lowest and negative for isotropic MLT (Case 1). Less values of pressure gradient $\text{grad}_x\ p$ correspond to less viscosity in the flow.

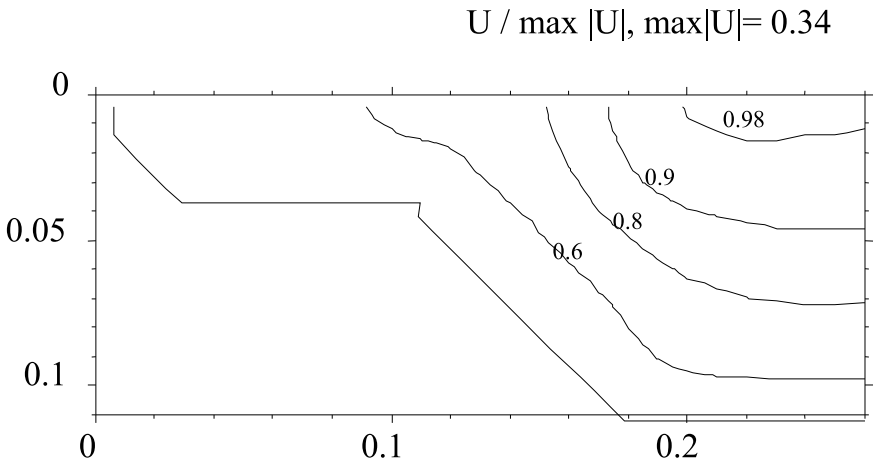

Fig. 5a. Prime velocity distribution for: $l_y = l_x, l_z = 0.67 l_x$

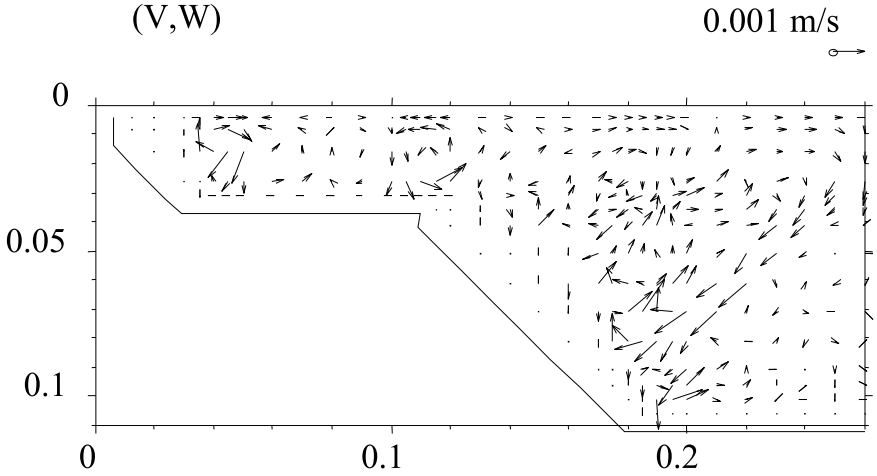

Fig. 5b. Secondary currents pattern for: $l_y = l_x, l_z = 0.67 l_x$; $Q_{\max} = 0.0126$ m/s

Mathematically it is obvious from x-momentum equation, where all viscous terms on the right hand side should balance pressure gradient terms on the left hand side. Inertia terms have a lower order of magnitude, and the gravitation term is constant. From a physical standpoint greater viscosity invokes greater pressure forces inside the flow. So the term $\mathrm{grad}_x\ p$ can be considered as an indicator of the total flow viscosity. It is interesting that in Case 4 the total viscous effect is stronger than in the isotropic Case 1. This effect can be explained by additional

viscous terms, which become nonzero when transversal components of MLT in LCS are different, as in Case 4 and Case 5 (see Table 1 and Eq. 16).

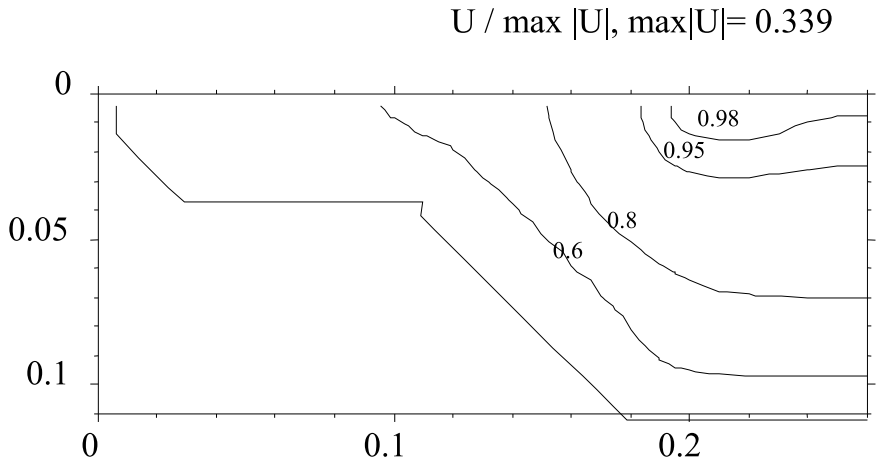

Fig. 6a. Prime velocity distribution for: $l_y = l_x, l_z = 1.45 l_x$

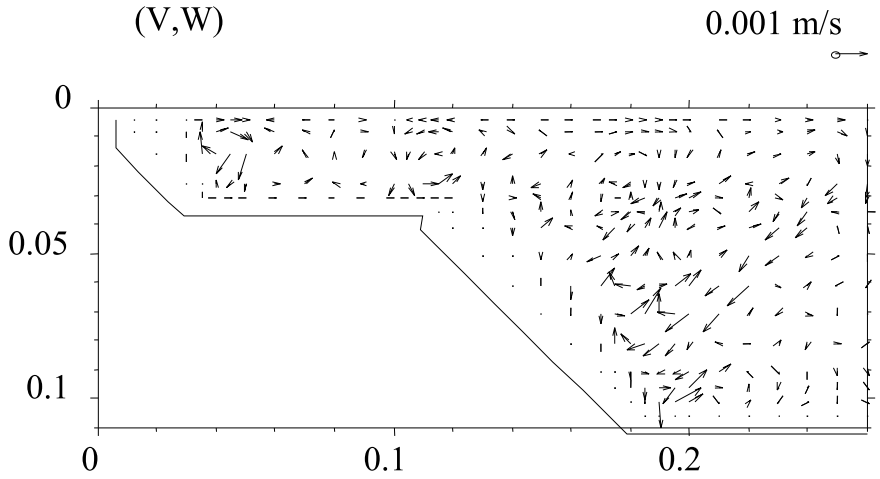

Fig. 6b. Secondary currents pattern for: $l_y = l_x, l_z = 1.45 l_x$; $Q_{\max} = 0.0103$ m/s

The prime velocity contours for $l'_z : l'_y = 0.67$ (Case 4) and $l'_z : l'_y = 1.45$ (Case 5) are very similar. Some differences occur only in the middle of the channel for larger velocity iso-lines (see Figures 5a and 6a). The secondary flow patterns for these two cases are also very similar. The most intensive secondary flow occurs for the ellipse narrowed in z-direction (Case 4), $Q_{\max} = 1.26$ cm/s. When l'_z

grows and reaches 1.45 l'_y (wide ellipse), the intensity $Q_{\max}$ decreases to 1 cm/s. In order to explain this result, let us consider any point located in the area above the inclined (45°) wall for these two cases. At this point both l_y and l_z have the same values and equal approximately to $0.5(l'_y + l'_z)$. Now, if l'_z grows from 0.67 l'_y to 1.45 l'_y, both mixing lengths l_y and l_z in GCS grow from 0.835 l'_y to 1.225 l'_y. It results in the growth of the effective viscosity (see Eq. 7) as well as the additional viscosity (see x–momentum equation) in both transversal equations.

The mixed components of MLT l^2_{yz}, describing additional viscosity, vanish for $l'_z = l'_y$, and then increase for two remaining cases (l'_z equals to 0.67 l'_y and 1.45 l'_y). This dynamics of additional viscosity is a plausible reason for changes in pressure gradient from 2.8 to –3.1, and then to 3.9 as l'_z goes up from 0.67 l'_y via 1 l'_y to 1.45 l'_y. The prime velocity distribution is about the same since the ratio of transversal viscosities has not changed. At a point in the main channel (in the area over the horizontal bed) the ratio of lateral eddy viscosities for cases 1 and 3 is equal to 0.85 : 1.25. This is the reason for some differences in the prime velocity distributions in the main channel.

A general conclusion can be stated based on the results of numerical simulations. The choosing of the main components of the MLT defines both the prime and secondary flow velocity distributions. The concept of MLH is very well known among civil engineers, then the 3D case of this hypothesis can be used by them without any problem. This 3D hypothesis is especially good for wide-open channels and rather simple cross sections. The reason is that only for these channels can one formulate the sub-models for the normal and shear turbulent stresses correctly.

7. Summary and Conclusions

1. The presented turbulence model takes into account differences between various components of the turbulent stress tensor. Contrary to the other models incorporating differential or algebraic equations for individual Reynolds stresses, it is fairly simple. It consists of two sub-models for shear and normal turbulent stresses.
2. The model is open, i.e., it allows us to use other sub-models for shear and normal turbulent stresses. The proposed sub-models take into account anisotropy in distributions of shear and normal turbulent stresses in open channel flows. They describe the streamwise velocity distribution in the compound channel flows with suitable accuracy for engineering applications. In case of a very sharp junction between the main channel and the flood plane or narrow channels it does not produce the proper velocity contour in the sub-surface layer. The sub-models allow obtaining of secondary motion generated by the turbulent shear stresses and normal stresses in open channel

flows. They give secondary flow patterns similar to those shown in monographs.

3. The numerical simulations show the possibilities of creating the prime velocity contours as well as the secondary flow patterns by changing the structure of the mixing length tensor. There is one limitation; the model gives the location of U_{max} at the water surface that is not usually true in some real open channels. This behaviour may be connected with the boundary conditions at the water surface or insufficient accuracy of the distributions of normal and shear Reynolds stresses in the surface sub-layer adopted in this study.
4. The model is very simple and easy to calibrate. It is particularly simple for channels with vertical sidewalls. For these channels all non-diagonal mixing length components in the global coordinate system are zeros. The calibration procedures need some information on turbulence structure of flows, especially the data on turbulence intensities and the structure of turbulent eddies. Today, these data are available only for simple flows but not for such complex flows as those in compound channels. The simple version of the model, using the spherical mixing length tensor, does not need any calibration procedure. Only the friction velocity and some flow parameters are needed.

References

Aris R. (1989), *Vectors, Tensors and the Basic Equations of Fluid Mechanics.*, Dover Publications, Inc., New York.

Cokljat D., Younis B. A. (1995), Second-order closure study of open-channel flows, *Journal of Hydraulic Engineering,* 121, 94–107.

Czernuszenko W., Rylov A. (2000), A generalization of Prandtl's model for 3D open channel flows, *Journal of Hydraulic Research*, 38, No. 2, 133–139.

Czernuszenko W., Rylov A. (2002), Modelling of 3D velocity field in open channel flows will appear, *Journal of Hydraulic Research*, 40, No. 2, 135–144.

Knight D. W., Yuen K. W. H., Alhamid A. A. I. (1994), *Boundary Shear Stress Distributions in Open Channel Flow,* [in:] *Physical Mechanisms of Mixing and Transport in the Environment*, Ed. Beven K., Chatwin P. C., Millbark J., J. Wiley.

Krishnappan G. B., Lau Y. L. (1986), Turbulence modeling of flood plain flows, *Journal of Hydraulic Engineering,* 112 (4), 251–266.

Launder B. E., Spalding D. B. (1974), The numerical computation of turbulent flows, *Computer Methods in Applied Mechanics and Engineering,* 3, 269.

Naot D., Nezu I., Nakagawa H. (1993), Hydrodynamic behavior of compound rectangular open channels, *Journal of Hydraulic Engineering,* 119 (3), 390–408.

Nezu I., Nakagawa H. (1993), *Turbulence in Open-Channel Flows*, A. A. Balkema, Rotterdam.

Nezu I., Rodi W. (1986), Open-channel flow measurements with a laser doppler anemometer, *Journal of Hydraulic Engineering*, 112, No. 5, 335–355.

Patankar S. V., Spalding D. B. (1972), A calculation procedure for heat, mass and momentum transfer in three-dimensional parabolic flows, *J. Heat Mass Transfer*, Vol. 15, 1787–1806.

Rastogi A. K., Rodi W. (1978), Predictions of heat and mass transfer in open channels, *Journal of the Hydraulics Division*, 104, No. HY3, 397–420.

Schlichting H. (1955), *Boundary Layer Theory*, McGraw Hill, London.